TU Delft

Delft University of Technology

Document Version
Final published version

Licence
CC BY

Citation (APA)
Bos, V., El Shenawy, M., Wesselingh, J., Steeneken, P. G., & Verbiest, G. J. (2026). Precise position feedback control of acoustically levitating objects by event-based vision. *Journal of Sound and Vibration*, *644*, Article 120040. https://doi.org/10.1016/j.jsv.2026.120040

Important note
To cite this publication, please use the final published version (if applicable).
Please check the document version above.

Copyright
In case the licence states “Dutch Copyright Act (Article 25fa)”, this publication was made available Green Open Access via the TU Delft Institutional Repository pursuant to Dutch Copyright Act (Article 25fa, the Taverne amendment). This provision does not affect copyright ownership.
Unless copyright is transferred by contract or statute, it remains with the copyright holder.

Sharing and reuse
Other than for strictly personal use, it is not permitted to download, forward or distribute the text or part of it, without the consent of the author(s) and/or copyright holder(s), unless the work is under an open content license such as Creative Commons.

Takedown policy
Please contact us and provide details if you believe this document breaches copyrights.
We will remove access to the work immediately and investigate your claim.

This work is downloaded from Delft University of Technology.

Journal of Sound and Vibration 644 (2026) 120040

Contents lists available at ScienceDirect

Journal of Sound and Vibration

journal homepage: www.elsevier.com/locate/jsvi

Precise position feedback control of acoustically levitating objects by event-based vision

Vincent Bos [a,*], Mohamed El Shenawy [a], Jasper Wesselingh [b], Peter G. Steeneken [a], Gerard J. Verbiest [a]

[a] Faculty of Mechanical Engineering, Delft University of Technology, Mekelweg 2, Delft, 2628 CD, the Netherlands
[b] ITEC BV., Jonkerbosplein 52, Nijmegen, 6534 AB, the Netherlands

ARTICLE INFO

Keywords:
Acoustic levitation
Feedback control
Event-camera

ABSTRACT

Acoustic levitation is a promising technique for contactless handling of small objects. However, for acoustic levitation in air, the positioning precision is usually too low and the response time too long for practical applications. In this work, we implement feedback control to reach high positioning precision. We realize real-time position monitoring at 2 kHz by an event camera and tracking algorithm. Using system identification and modeling, we design a PID controller for position feedback that can stabilize the position along a single axis. The controller is shown to reduce the particle response time to 0.06 s and reach a closed-loop RMS horizontal positioning error of 19 μm, outperforming the state of the art. With the feedback control, the positioning precision of acoustic levitation is brought into a regime comparable to the positioning performance of additive manufacturing methodologies.

1. Introduction

Acoustic levitation is very promising for handling of small particles or small amounts of liquid in chemistry [1,2], biophysics [3], microassembly [4,5] and additive manufacturing [6]. It has been shown that particles ranging from tens of micrometers [7] up to half the acoustic wavelength can be levitated [8]. Using sophisticated methods, even particles much larger than the wavelength can be levitated [9]. Using phased arrays, a levitated particle can be moved and its orientation can be controlled [10].

However, challenges are to be overcome to unlock the full potential of acoustic levitation. Disturbances arising from airflow and temperature fluctuations heavily affect the position of the levitated particle, as the stiffness of acoustic traps [10] is low compared to contact-based positioning systems. In addition, the low damping resulting from air drag results in high ring-down times (about 10 s [11]). Consequently, any motion of the levitated particle due to a disturbance does not quickly damp out. As the disturbances cause high amplitude and long-lasting vibrations due to low stiffness and damping, the positioning precision is poor [10].

We could think of several approaches that potentially could improve the precision and accuracy of a levitated particle, although these approaches are not validated yet. First, one can increase the acoustic field stiffness by increasing the acoustic pressure or frequency. However, this only works to some extent, as new limitations emerge due to nonlinearities in the acoustic field [12]. Second, shielding the levitated particle from the environment could potentially remove disturbance from surrounding airflow. However, shielding might be impractical for handling applications. Moreover, the generated heat and convection [13,14] in the levitator still

* Corresponding author.
E-mail address: v.bos@tudelft.nl (V. Bos).

https://doi.org/10.1016/j.jsv.2026.120040
Received 10 October 2025; Received in revised form 31 July 2026; Accepted 1 August 2026
Available online 9 August 2026
0022-460X/© 2026 The Authors. Published by Elsevier Ltd. This is an open access article under the CC BY license (http://creativecommons.org/licenses/by/4.0/).

forms a source of disturbances, beside the acoustic streaming that creates air flow around the particle [15,16]. Third, using a different gas than air might improve stiffness and damping [11,17], but requires a more advanced setup and limits the range of applications.

Recently, a different approach was proposed by Andrade et al. [18]. They reduced the response time and vibrations of a levitated particle using feedfoward control. The controller filters the levitation trajectory using knowledge of the levitation dynamics. Yet, feedforward control is limited as it cannot deal with unexpected or random disturbances. Therefore, an active feedback system would be a preferred solution as it can suppress motion caused by disturbances [19]. Bos et al. [11] showed that the response time can be drastically reduced using active damping. Here, a laser Doppler vibrometer was used to measure the particle velocity in order to provide velocity proportional feedback. Using this approach, the response time was reduced from $9.7\,\mathrm{s}$ to $0.01\,\mathrm{s}$. Nevertheless, a vibrometer can measure the particle motion only at a single spot and can stabilize motion only along a single axis. Therefore, implementing this technique for multiple levitating particles along multiple axes may be impractical, as each particle and axis would need its own laser Doppler vibrometer, that is continuously aimed at the particle.

Vision systems have proven themselves in many applications for tracking the position and orientation of objects of various shapes [20]. Objects may be located throughout the field of view and lenses can be used to adapt to the object size. For example, Willert [21] shows how to track numerous spherical particles with a diameter of $10\,\mu\mathrm{m}$ in a $44 \times 5.9\,\mathrm{mm}$ field of view and perform particle image velocimetry. Several works describe various implementations of vision systems operating in real-time. Here, we consider real-time vision systems that both record and analyze each frame from the camera output as fast as possible after it is captured. For example, Johnson [20] describes simultaneous tracking of multiple vehicles and pedestrians using a static camera. The camera records frames of 768x576 pixels in color at a frame rate of 50 frames per second (fps). The frames are processed in real-time on a Pentium D desktop computer using the Open Source Computer Vision library (OpenCV). Furthermore, Ye [22] applies a vision system for feedback control. He controls the position of a patterned surface in one direction. The camera takes a picture of the surface, which is compared to a reference image in order to determine the positioning error. Subsequently, a controller aims to move the surface to the correct location.

Although promising, current vision systems still have limitations. The sensor data has to be processed in real-time to extract the object position. As the camera covers a wide field of view, an enormous amount of data [23] is generated per measurement-frame. For example, Delbruck et al. reported that a vision system operating at a frame rate of $1\,\mathrm{kHz}$, having 128x128 monochrome 8-bits gray pixels, produces a data stream of 16 Mbytes/s. Processing this data in real-time is still a challenge, and usually the limiting factor of real-time vision systems. In the childhood of visual servoing, Corke [24] already wrote: “visual servoing has a relatively low sample rate, significant latency (one or more sample intervals) and coarse quantization [24]”. Those limitations are related to the huge amount of data that is generated. As sensor sample rate, latency and quantization largely determine the performance of a feedback system, using vision in feedback control is still challenging.

The main issue in conventional frame-based vision for object tracking is that the camera generates a lot of data of which only a small part is useful. The object usually takes only a small part of the image, and therefore redundant background information dominates the data stream. This requires a processing step that distinguishes the object from the background and thereby reduces the amount of data. Subsequently, the actual object tracking step may take place using the much lighter data stream.

Lichtsteiner et al. [25] have described an event-based camera that does not gather background data. This camera only registers changes in light intensity. Therefore, only the contours of moving objects are registered. As background data is not registered, the data flow is tremendously reduced for small moving objects. For example, in a calm scenario in which 8% of the pixels is active (changing over time instead of being static background), the data stream of an event camera is 1% [26] compared to that of the aforementioned 8-bit monochrome frame-based camera. Moreover, no background-subtraction is required in the image processing. This camera is called an event-camera or silicon retina, as it mimics the human eye.

Because processing data from an event camera is computationally cheap (compared to frame-based camera), it can be performed on a CPU in real-time as was shown by Ni et al. [27]. Willert [21] reports an event-based vision system that has a sample rate of $10\,\mathrm{kHz}$ and a latency of $200\,\mu\mathrm{s}$ [21,28]. Therefore, event cameras are promising candidates for tracking the position of levitated particles in real-time.

In this work, we show feedback control of a levitated particle using an event camera as position sensor. The event camera is connected to a desktop computer which performs the particle tracking on the event data. The position information is sent to a system-on-module (SOM) with a feedback controller to update the acoustic field and thereby improve the positioning of the levitated particle. Using the feedback controller, we reduce the particle vibrations and decrease the particle response time. Finally, we validate the performance using a conventional frame-based high-speed camera.

This paper is organized as follows. First, we introduce the acoustic levitator and discuss how we determine the position of a levitated particle using an event camera. Subsequently, we perform system identification in order to identify the dynamics of the complete system. This includes the amplitude and phase response of the levitated particle, the sensor (event camera) and the control unit (SOM). Then, we design a feedback controller using this information. Finally, we evaluate the performance of the feedback controller by quantifying its ability to isolate the levitated particle from vibrations, characterized by the positioning error. Furthermore, we test the ability to move the levitated particle quickly using a step-response, characterized by its settling time.

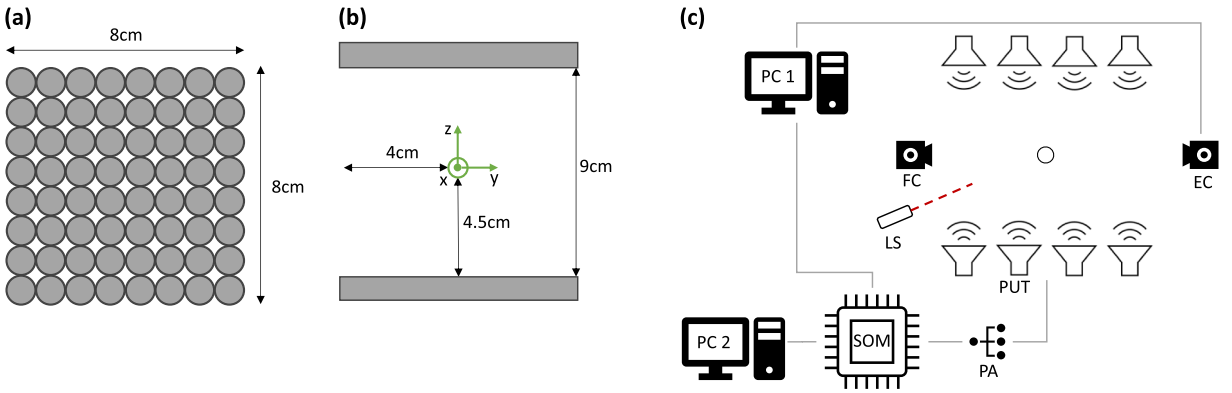


Fig. 1. The acoustic levitation setup. **a**) Top view transducer array **b)** Side view transducer array including the coordinate system in green at the levitation location **c)** Setup schematic. SOM: System-on-module - PA: Power amplifiers - PUT: Piezo-electric ultrasonic transducers - LS: Light source (laser) - EC: Event-based camera - FC: Frame-based camera - PC 1: Desktop PC for real-time object tracking - PC 2: Desktop PC for data acquisition. - Note that the light source is located beside the camera although this orientation could not be shown in the schematic. (For interpretation of the references to colour in this figure legend, the reader is referred to the web version of this article.)

2. Method

2.1. Acoustic levitation setup

The acoustic levitator consists of two opposing piezoelectric ultrasound transducer (PUT) arrays. Each array consists of 64 Murata MA40S4S transducers with a diameter of 1 cm. The transducers are arranged in a square array that measures 8 times 8 cm, and the arrays are at a vertical distance of 9 cm apart, as shown in Fig. 1. We levitate a white polyethylene (PE) spherical particle which has a diameter of 0.55 ± 0.05 mm and a density of 1300 kg m^{-3}. By electronically controlling the transducer signals an acoustic trap is generated at focus point $\mathbf{r}_t$ ($\mathbf{r}_t = [x_t, y_t, z_t]$), which is located exactly in the middle of the two transducer arrays. Because the acoustic trapping force is large enough to overcome gravity, the PE particle levitates at that point. We create a z-trap (or standing wave as introduced by Marzo et al. [10]) which features high vertical stiffness but also stiffness in both horizontal directions. The location of the trap can be controlled in both horizontal and vertical direction by changing the location of the focus point $\mathbf{r}_t$, by controlling each individual transducer signal. In Suppl. Sec.(5.1) we further explain how the transducer phases are calculated to generate the acoustic trap.

The acoustic field is controlled by system-on-module (SOM), which calculates the individual transducer signals for a given trap location $\mathbf{r}_t$. 128 voltage signals are generated at the output of the SOM, which are subsequently amplified by 128 power amplifiers (PA) to a peak-to-peak voltage of 28.6 V. Those 128 signals drive the Murata ultrasound transducers. Fig. 1 gives an overview of this setup, and in Suppl. Sec.(5.1.2) we further describe the transducer signal generation.

We use a conventional camera to validate the motion of the feedback-controlled levitated particle. We combine this frame-based high-speed camera (FC) with a telecentric lens, and record at a frame rate of 200 frames per second (fps). This camera features a pixel-size of 13.7 µm and the lens has a magnification of one. To determine the position of the sphere for each frame, we use the 'imfindcircles' function in Matlab, which uses a Circular Hough Transform based algorithm to find and fit a circle for each image. For circles larger than 5 pixels, this algorithm can yield sub-pixel resolution [29].

2.2. Position measurement

In this section we explain how we determine the position of the levitated particle in real-time. First, we explain how we implemented the event camera and optical arrangement. Second, we explain how we determine the particle position from the generated data using a tracking algorithm.

In Fig. 1(c) a schematic overview of the setup is shown. The event camera (EC) is connected to a desktop computer (PC 1) which performs real-time object tracking. The position information is sent to the SOM in which the feedback control algorithm is implemented. A photo of the setup is shown in Suppl. Fig. 18, indicating the event camera, the frame-based camera and the levitator.

We use the EVK4 event camera, which is commercially available from Prophesee. This camera has 1280x720 pixels and can be connected via USB 3.0. The event camera has a pixel size of 4.86 µm, which is converted to an effective pixel-size of 6.48 µm through the telecentric lens (which has a magnification of 0.75). The object is illuminated by a red laser that has a spot-size of about 4 mm and is located beside the frame-based camera (as shown in Fig. 1), pointing just next to the lens mounted on the event-camera. As a result of the spherical shape of the particle, a small part of the laser beam is reflected into the event camera sensor. This causes a small bright spot at one side of the sphere that facilitates tracking the particle with the event camera sensor, shown in Fig. 2. The working principle of the event camera itself is explained in Suppl. Sec. 5.4.



Fig. 2. Event generation for a levitated sphere illuminated from the back side (as shown in Fig. 1(c)). The white area marks generated events (Explained in more detail in Suppl. Sec. 5.4.1).

We use the 'Spatter tracking' algorithm which can track arbitrary shaped objects and is freely available from Prophesee, the camera manufacturer [30]. The algorithm first interfaces and buffers the incoming data from the camera and then determines the object location from the buffered event data. The object location is determined at a sample rate of 2 kHz and sent to the SOM via udp. In Suppl. Sec. 6 the tracking algorithm is explained and the tracking settings used during experiments are listed.

2.3. Controller layout

Here, we explain the implementation of feedback control. First, we explain how we can use the acoustic trap to exert a force on the levitating particle. Second, we model the dynamics of the levitated particle and third we describe the controller layout.

By setting the location of the acoustic trap x_t (the x-coordinate of the focus point $\mathbf{r}_\mathrm{t}$) different from the particle location x_p (see Fig. 3(a)), we can exert a horizontal force on the particle. In the following, we will only implement feedback to control the horizontal motion x_p. Note that the procedure can be extended to control more degrees of freedom.

Fig. 3(b) shows the control scheme that we use. Here, the reference location x_r is the location where we aim to position the levitated particle. The error signal e equals the difference between the reference location x_r and the measured location of the particle x_p. The controller C acts upon this error signal e and calculates the new trap location x_t. Disturbances acting on the levitated particle like airflow and transducer fluctuations are modeled as a process disturbance d. The disturbance d and the new trap location x_t both are input to the plant P (the levitated particle).

In order to understand the dynamics of the levitated particle (plant P), we model it as a mass-spring-damper model (details in Suppl. Fig. 1). The resulting equation of motion is

$$\ddot{x}_\mathrm{p} + 2\zeta\omega_\mathrm{n}\dot{x}_\mathrm{p} + \omega_\mathrm{n}^2(x_\mathrm{p} - x_\mathrm{t} - d) = 0, \tag{1}$$

where ω_n equals the eigenfrequency of the levitated particle in $\mathrm{rad\,s^{-1}}$ and ζ equals the damping ratio. In the following definition of the plant P (Eq. (2)), the trap displacement x_t is the only external input ($d = 0$) as disturbance d interacts in the same manner as trap displacement x_t (according to Fig. 3(b)). The transfer function P of the plant is found from the Laplace transform of Eq. (1):

$$P(s) = \frac{X_\mathrm{p}(s)}{X_\mathrm{t}(s)} = \frac{\omega_\mathrm{n}^2}{s^2 + 2\zeta\omega_\mathrm{n}s + \omega_\mathrm{n}^2}, \tag{2}$$

where we use a capital to indicate the Laplace transform of each time signal ($X(s) = \mathcal{L}\{x(t)\}$).

We implement feedback control in order to reduce vibrations (due to disturbance d) of the levitated particle and shorten the settling time T_s. The 5%-settling time equals

$$T_\mathrm{s} \equiv -\ln(0.05)\frac{1}{\zeta\omega_\mathrm{n}} \tag{3}$$

which indicates the time after which vibrations remain smaller than 5% of the initial step. We implement a Proportional-Integral-Derivative (PID) controller [19,31], which can stabilize the particle and also reduce the settling time. The controller C has the following layout:

$$C(s) = k_\mathrm{p}\left(H_\mathrm{m}(s)\cdot(1 + \tau_\mathrm{d}s) + \frac{1}{\tau_\mathrm{int}s}\right) \tag{4}$$

where k_p equals a proportional gain and the time-constants τ_int and τ_d are related to respectively the integration and derivative action. Each time-constant τ_i is related to a frequency f_i according to the following relation:

$$\tau_i = \frac{1}{2\pi f_i} \tag{5}$$

and $H_\mathrm{m}(s)$ equals a N_m-point moving average filter (details in Suppl. Sec. 3.1.8).

We design the controller by loop-shaping the frequency response [19]. Here, the frequencies f_i are used as tuning parameters of the controller design. This method is very convenient to use because later we identify the plant P in the frequency domain. The actual controller design is explained in Section 3.3.

3. Results

In this section we present the results of the implementation of feedback control. First, we identify the open-loop dynamics of the levitated particle to determine the system parameters f_n, ζ and the delay τ_d. Using this information, we design a feedback controller and finally we examine the performance of the feedback-controlled particle.

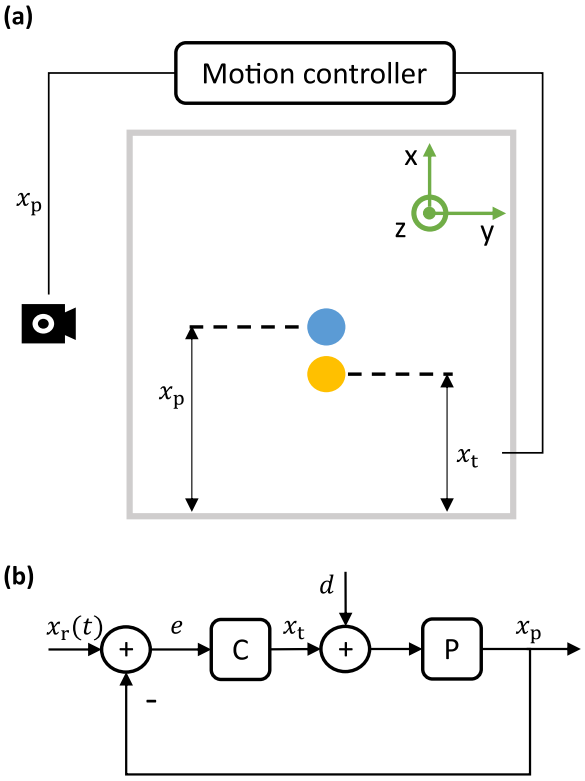


Fig. 3. Feedback implementation - x_p: particle position - x_t: trap position - x_r: reference position - e: error signal - d: disturbance signal - **a)** Trap position for feedback. The levitator is shown from top, the grey square indicates the outer boundary of the transducer array and the coordinate system is shown in green. - **b)** Block diagram of the feedback system. C: Controller - P: Plant (levitated particle, defined in Eq. (1)). (For interpretation of the references to colour in this figure legend, the reader is referred to the web version of this article.)

3.1. Identification of the plant

First, we identify the dynamics of the system in the open-loop configuration. This includes the levitated particle as well as the sensor (event camera and corresponding hardware). We move the acoustic trap in horizontal direction according to the reference signal $x_r(t)$, while we monitor the particle movement $x_p(t)$ with the event camera. We record both the reference signal $x_r(t)$ and the measurement signal $x_p(t)$ at the SOM, such that we can determine the relation between the two using FFT analysis. We use a multisine signal as reference signal $x_r(t)$, as this contains a wide band of frequencies. The multisine signal has a frequency resolution of 0.25 Hz, a frequency range of 0.25 Hz to 60 Hz and a maximum amplitude of 0.33 mm. The multisine signal is constructed according to Eq. (6)

$$x_r(t) = \sum_{i=1}^{N} A_i \sin(\omega_i t + \varphi_i), \tag{6}$$

where A_i equals the amplitude, ω_i the frequency and φ_i the phase offset of each signal component. The parameter values used in Eq. (6) are listed in the Suppl. Table 1.

In Fig. 4 we show the result of this identification method. We show the ratio of the measured particle movement x_p over the trap movement x_t along the reference signal x_r. We determine this ratio by dividing the frequency spectrum of the measured output $X_p(j\omega)$ over the frequency spectrum of the input signal $X_r(j\omega)$ (time domain data is presented in Suppl. Sec. 2.1.1). Subsequently, we fit, in the frequency domain, Eq. (7) to the measured output-over-input ratio $\frac{X_p(j\omega)}{X_r(j\omega)}$:

$$H(s) = \frac{X_p(s)}{X_r(s)} = \frac{\omega_n^2}{s^2 + 2\zeta\omega_n s + \omega_n^2} \cdot e^{-\tau_d s}. \tag{7}$$

Eq. (7) is derived from Eq. (2) (shown in Suppl. Sec. 1.2) but has an additional time delay τ_d to account for the time delay present in the measurement system. From the fit (the blue line in Fig. 4) we find the model parameters f_n, ζ and τ_d, which are listed in Table 1.

Table 1
Open-Loop system identification: Characteristic dynamic quantities of the levitated particle (the plant P in Fig. 3). Values are deduced from Fig. 4.

Quantity	Value	Description
ζ	1.4×10^{-2}	Damping ratio
f_n	1.2×10^{1} Hz	Eigenfrequency
τ_d	5.5 ms	Time delay

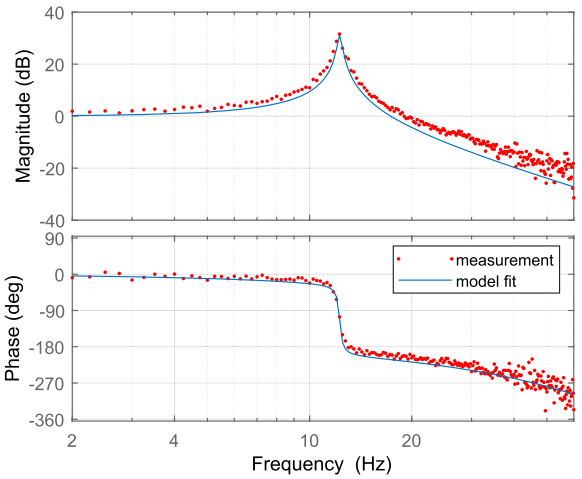


Fig. 4. Identification of the plant (P in Fig. 3) in the frequency domain as described in Section 3.1. We show the data in the frequency domain using the Bode diagram of $H(\mathrm{j}\omega) = \frac{X_\mathrm{p}(\mathrm{j}\omega)}{X_\mathrm{r}(\mathrm{j}\omega)}$, where $X_\mathrm{p}(\mathrm{j}\omega)$ is the frequency domain transformed measurement data of the particle displacement and $X_\mathrm{r}(\mathrm{j}\omega)$ the transformed data of the reference signal along which we displace the trap. The data is fit to the model defined in Eq. (7). This yields fit values $f_\mathrm{n} = 1.2 \times 10^{1}$ Hz, $\zeta = 1.4 \times 10^{-2}$ and $\tau_\mathrm{d} = 5.5$ ms. The magnitude axis is expressed in dB: $20 \log_{10} |H|$.

3.2. Identification of disturbances

Second, we identify the particle vibrations originating from disturbances. To do so, we fix the trap position ($x_\mathrm{r}(t) = 0$) while we record the particle movement with a high-speed frame-based camera (FC in Fig. 1(c)). The vibrations present originate from disturbance sources like air flow around the particle and random trap movement. This trap movement can be due to heating of the transducers or temperature fluctuations in the levitator, which affect the acoustic wavelength and thus the location of the trap (see Suppl. Sec. 5.1.1). As these phenomena excite the levitated object, we model them as a process disturbance [19] d in Fig. 3(b). Using this model, the vibrations of the particle x_p are related to the disturbance source according to $X_\mathrm{p}(s) = P(s) \cdot D(s)$, as the reference signal $x_\mathrm{r}(t)$ equals zero in this situation. Note that in this experiment there is no feedback applied ($C = 0$).

We show in Fig. 5 the Power Spectral Density (PSD) of the particle movement, which we determine in Matlab using the Pwelch function. In Fig. 5 we can see that the disturbance source has high PSD at low frequencies, while it decreases for higher frequencies. Clearly, a resonance is visible at 1.2×10^{1} Hz, due to the fact that we plot the vibration PSD corresponding to the product $\mathrm{PSD}_{X_\mathrm{p}} = |P(\mathrm{j}\omega)|^2 \cdot \mathrm{PSD}_D$ (where $\mathrm{PSD}_{X_\mathrm{p}}$ is the PSD of X_p). The eigenfrequency f_n of the levitated particle corresponding to horizontal motion equals 1.2×10^{1} Hz, and is therefore visible in the particle response shown in Fig. 5.

The PSD corresponding to vertical motion (z) in Fig. 5 also shows a peak at 1.2×10^{1} Hz. We assume that this is due to coupling of horizontal (x) motion to vertical (z) motion, as explained in Suppl. Sec. 1.3. The PSD of vertical motion shows a second peak at 40 Hz, which corresponds to the resonance of vertical motion as shown in Suppl. Fig. 6. The motion is excited by disturbance source d, resulting in particle motion in vertical direction ($\mathrm{PSD}_{Z_\mathrm{p}} = |P_z(\mathrm{j}\omega)|^2 \cdot \mathrm{PSD}_D$) as shown in Suppl. Fig. 11.

3.3. Controller design

We implement feedback control to reduce the vibrations σ and reduce the settling time T_s of the levitated particle. The vibrations arise from disturbances (d in Fig. 3(b)) and movement of the acoustic trap location (x_r in Fig. 3(b)). We design the controller according to the method called loop-shaping [19]. This method uses the frequency spectrum representation of the feedback system, which is very convenient as we also identified the system in the frequency domain.

The first design parameter of the controller that we set is the phase margin (PM). The phase margin is [32] the amount by which the phase of the open-loop response ($L(s) = C(s) \cdot P(s)$) is more positive than $-180°$, evaluated at the frequency where the magnitude

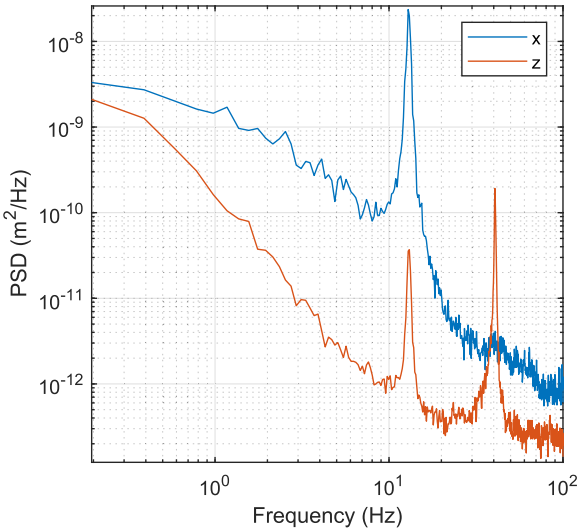


Fig. 5. Disturbance vibration spectrum: The PSD shows vibrations caused by the disturbances acting on the levitated particle: $\mathrm{PSD}_{x_p} = |P(\mathrm{j}\omega)|^2 \cdot \mathrm{PSD}_D$ (according to the model shown in Fig. 3(b)) and $\mathrm{PSD}_{z_p} = |P_z(\mathrm{j}\omega)|^2 \cdot \mathrm{PSD}_D$ according to the model shown in Suppl. Fig. 11. In this experiment, the location of the acoustic trap is constant: $x_t(t) = z_t(t) = 0$.

Table 2
Controller design: Settings of the implemented PID controller.

Qty.	Value	Description	Reference
k_p	0.35	Proportional gain	Eq. (4)
f_c	19 Hz	Unity gain cross over frequency	Suppl. Fig. 9b
f_{int}	23 Hz	Integrating action	Eq. (4)
f_d	3.6 Hz	Differentiating action	Eq. (4)
PM	35°	Phase margin	Suppl. Fig. 9b
GM	8.4 dB	Gain margin	Suppl. Fig. 9b
T_s	0.1 s	Settling time (5%)	Eq. (3)
T_m	0.4 ms	Sample period controller	Suppl. Eq. 34
N_m	4	Window size moving average	Suppl. Eq. 34
f_{cm}	282 Hz	Corner frequency moving average	Suppl. Eq. 34

of open-loop response $L(s)$ equals one (the unity-gain cross over frequency f_c, see Suppl. Sec. 3.1.2). We choose the phase margin to be 35°, as this provides us a decent stability margin and damping ($\zeta \approx \mathrm{PM}/100$). We set the phase margin by the differentiation action f_d. Second, we require the open-loop gain $L(s)$ to be larger than −6 dB for frequencies lower than the natural eigenfrequency $f_{\text{n-x}} = 1.2 \times 10^1$ Hz. This enables the particle to properly follow a reference signal $x_r(t)$. We realize this using the controller parameter f_{int}, which sets the integral action. Third, we choose the proportional gain k_p as high as possible to provide additional stiffness. In Table 2 the controller parameters, stability margins and performance indicators are listed. Furthermore, in Suppl. Sec. 3.1 additional details concerning the controller are provided like the modeled open-loop response ($L(s) = C(s) \cdot P(s)$) of the compensated system (Suppl. Fig. 9b).

In the acoustic field, there is a coupling between vibrations in the horizontal and vertical direction [33]. This becomes clear from Fig. 5 where a vibration power peak occurs for vertical motion z_p at the horizontal eigenfrequency $f_{\text{n-x}}$. We identify this coupling further in Suppl. Sec. 2.3. We apply active damping on vertical particle motion to reduce vibrations in this direction. This active damping reduces the vibration power of vertical motion, and limits the coupling effects between horizontal and vertical motion. The implementation is shown in Suppl. Sec. 3.2.

3.4. Closed-loop performance

In Fig. 6 we show the performance of the feedback-controlled particle. In Fig. 6(a) we show (as in Fig. 4) the frequency response for multisine excitation, for the open-loop and closed-loop system. Here, we move the reference location x_r according to the multisine signal (Eq. (6)) and monitor the particle movement with the event camera.

The closed loop system shows a reference-tracking bandwidth B_{rt} (Table 3) of 5.0×10^1 Hz, which is the highest frequency with which we can substantially move the particle, determined from the −6 dB crossing of the response shown in Fig. 6(a). Note that this bandwidth is higher than the open-loop bandwidth of 2.6×10^1 Hz. Moreover, the resonance of the closed-loop system has a

Table 3
Performance of the open-loop (OL), closed-loop (CL) and modeled closed-loop system. *for the closed-loop system, ζ is calculated from the overshoot [32] as no oscillations were present in this experiment. † The 'Source' column indicates the related figure for the open-loop (OL) and closed-loop (CL) column. Material related to the modeled performance (model CL column) is provided in Suppl. Sec. 3.1. ‡ The reference tracking bandwidth is determined from the −6 decibel crossing in Fig. 6(a), indicating an output-over-input amplitude ratio $\left|\frac{X_p(j\omega)}{X_r(j\omega)}\right|$ of 0.7.

Quantity	OL	model CL	CL	Source†	Description
T_s	2.3 s	0.1 s	6×10^{-2} s	Fig. 6(b) & 6(c)	Settling time (5%)
ζ	1.4×10^{-2}	0.35	0.62*	Fig. 6(a) & 6(f)	Damping ratio
B_{rt}	2.6×10^{1} Hz	3.2×10^{1} Hz	5.0×10^{1} Hz	Fig. 6(a)	Reference tracking bandwidth‡
σ_x	1.0×10^{-4} m	2.5×10^{-5} m	1.9×10^{-5} m	Fig. 6(d)	Horizontal RMS error
σ_z	2.3×10^{-5} m	7.2×10^{-6} m	2.0×10^{-5} m	Suppl. Fig. 13	Vertical RMS error

magnitude of only 4 dB, which is much lower than the open-loop resonance that has a magnitude of 40 dB. This implies that the closed-loop system has more damping compared to the open-loop system.

In Fig. 6(d) we show the vibration PSD of the open-loop and closed-loop system. For this experiment, we use a constant reference signal ($x_r = 0$) and monitor the particle vibrations, just as shown in Fig. 5. We record the particle motion with the frame-based camera (FC) and determine the PSD.

The vibration PSD is reduced especially at frequencies lower than 1 Hz and at the resonance frequency (1.2×10^{1} Hz). The total positioning error is quantified using the root-mean-squared (RMS) vibration level σ, which is defined [19] as:

$$\sigma = \sqrt{\sum_{i=1}^{N} P_i(f_i)\Delta f}, \tag{8}$$

where $P_i(f_i)$ equals the vibration PSD at frequency bin f_i, and Δf equals the frequency bin size. This positioning error is reduced from 1.0×10^{-4} m to 1.9×10^{-5} m for horizontal motion. The PSD of vertical motion is shown in Suppl. Sec. 4.1, and the coupling between horizontal and vertical motion is further investigated in Suppl. Sec. 1.3. The positioning error in vertical direction is changed from 2.3×10^{-5} m to 2.0×10^{-5} m.

Finally we evaluate the performance of the feedback-controlled particle using a square wave reference signal $x_r(t)$. In this experiment we use the event camera in the feedback loop and use the frame-based camera to record the particle motion for performance evaluation. In Fig. 6(b) we show the particle response for the case that we apply no feedback. Here, the particle shows overshoot of about 0.4 mm after the reference location x_r changes, which is almost equal to the reference location jump value. Subsequently, the particle remains vibrating during the settling time T_s, which is about 2.3 s. After this period, the particle remains vibrating and also the mean value remains drifting over time. Fig. 6(e) provides a detailed view on a short time interval of the signal shown in Fig. 6(b), on the short time span just after the reference location x_r is changed. Here we can clearly observe the long-lasting harmonic vibrations of a highly under-damped system.

In Fig. 6(c) we repeat the same experiment while feedback control is active. Here, after the reference location x_r changes, the particle follows the reference location x_r and remains close to this value as long as the reference location x_r remains in place. After the particle is settled, it hardly shows vibrations or drift.

In Fig. 6(f) we zoom in on the time span just after the reference location x_r is changed. Here, we observe that the particle shows only little overshoot (0.075 mm), oscillates hardly and quickly settles within 6×10^{-2} s. In Table 3 the performance indicators of the levitated particle are listed for the uncontrolled and the controlled situation.

4. Discussion

We demonstrated in Fig. 6(b) and (c) that position feedback can reduce the settling time of a levitated object. As listed in Table 3, the settling time was reduced from 2.3 s to 6×10^{-2} s. Moreover, the levitated particle settles at the location of the reference signal $x_r(t)$, also after the reference signal value changes (shown in Fig. 6(c)). The particle vibrations in the controlled direction are drastically reduced from $\sigma_x = 1.0 \times 10^{-4}$ m to $\sigma_x = 1.9 \times 10^{-5}$ m, as elaborated in Fig. 6(d). To our knowledge, this outperforms the state-of-the art, which typically reports a repositioning error of 5×10^{-5} m to 7×10^{-5} m [10,34].

The behavior of the feedback-controlled levitated particle is close to the behavior predicted by the model (Fig. 3), as shown in Table 3. Therefore, the settling time T_s and vibration amplitude σ_x can be predicted using a simple linear model (as explained in Suppl. Sec. 1.4).

Compared to stabilization approaches reported in literature (feed-forward compensation [18] and active damping [11]), our implementation of position feedback has several new capabilities. First of all, the steady state position of the levitated object is aligned with the desired position using position feedback (Fig. 6(c)). This implies that the positioning accuracy is improved. Second, vibrations due to disturbances (σ_x) are suppressed (Fig. 6(d)), such that the positioning precision is improved. Third, the reference

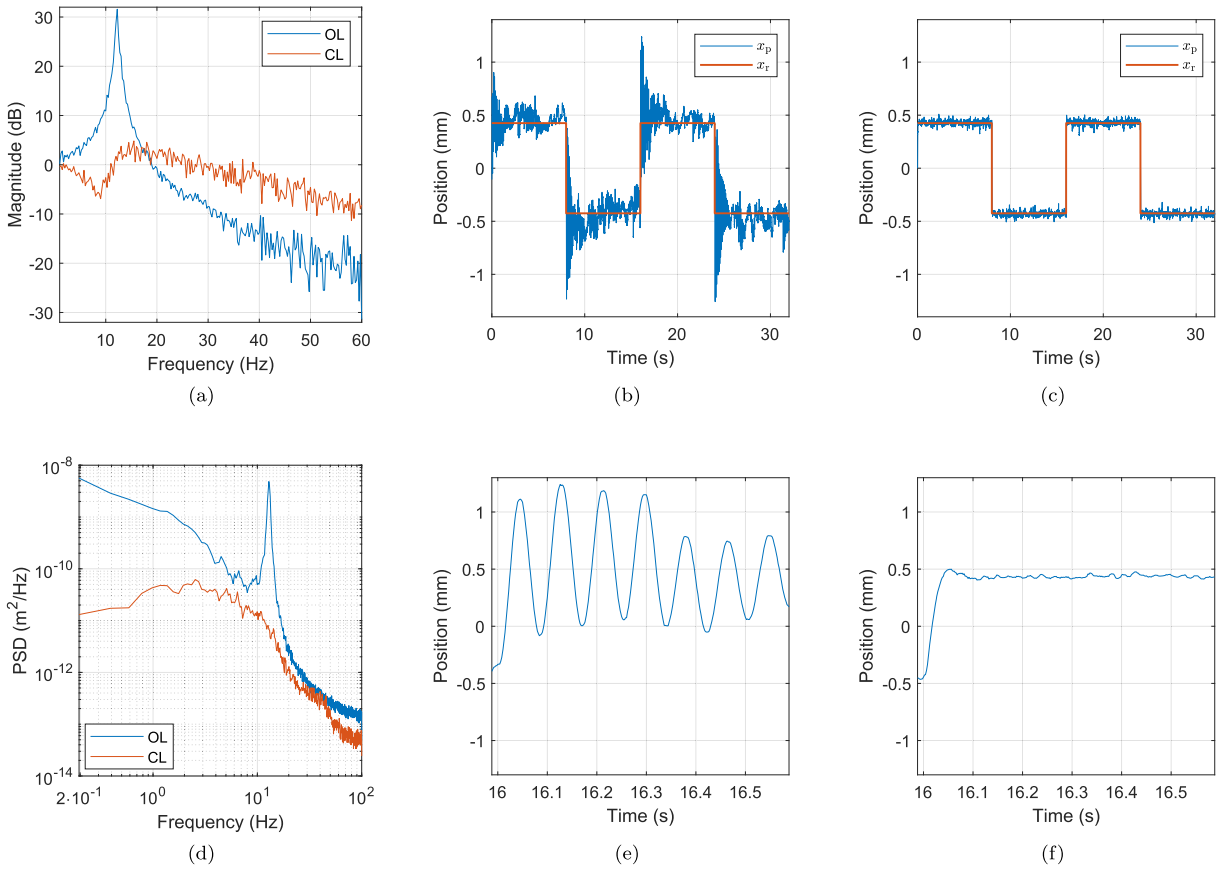


Fig. 6. Performance of the feedback control system **a)** Bode diagram showing the output-over-input ratio of $H(\mathrm{j}\omega) = \frac{X_p(\mathrm{j}\omega)}{X_r(\mathrm{j}\omega)}$, experimentally determined using a multisine reference signal $x_r(t)$ (like Fig. 4). Magnitude in dB: $20\log_{10}|H|$. - **b)** Particle response $x_p(t)$ to a square wave reference signal $x_r(t)$ - No feedback is applied. - **c)** Particle response $x_p(t)$ to a square wave reference signal $x_r(t)$. In this case, feedback is applied. - **d)** Disturbance vibration spectrum: The PSD shows vibrations caused by the disturbances acting on the levitated particle. In this experiment, the reference signal is constant: $x_r(t) = 0$. OL: open-loop system CL: closed-loop system. - **e)** Detailed view of a short time interval of Fig. 6(b) - **f)** Detailed view of a short time interval of Fig. 6(c).

tracking bandwidth B_{rt} is increased (Table 3), increasing the frequency with which we can position the particle. Nevertheless, feedforward compensation [18] and active damping [19] could still be applied in combination with position feedback [19]. In this way, vibrations related to the reference signal $x_r(t)$ can be further suppressed.

Illumination and event generation

Usually, an object is illuminated from the front for visual tracking. Using an event camera, this method generates positive events at the front and negative events at the rear of the illuminated object (shown in Suppl. Fig. 21). Those two zones with high event rate can be tracked separately, from which the object midpoint can be determined. However, in this work we used a laser to illuminate the levitated sphere from the back side. In this way, both positive and negative events are continuously generated at the sphere's side. This allows to remove the negative events using the biases, reducing the event-rate and thus the computational load. Moreover, there is only a single spot to be tracked, which remains visible even when the particle is not moving. Therefore, this type of illumination makes the tracking simpler and more reliable. We further note that the reported RMS positioning error of $\sigma_x = 19\,\mu\mathrm{m}$ is larger than the pixel size of $6.48\,\mu\mathrm{m}$, and therefore we assume the optical system not to be the limiting factor for the precision in the current situation.

Performance event camera versus frame-based camera

To position the performance of the motion tracking shown in this work with respect to the state-of-the-art, we compare it to some configurations reported in literature, listed in Table 4. Listed items give an indication of typical performance for different hardware implementations. The systems using a frame-based camera were selected by Ye [22] as being representative for the state of the art. The performance of a vision system for motion tracking can be indicated using the two performance-indicators K_{lat} and K_{smp}:

Table 4
A selection of vision tracking systems reported in literature, giving an indication of typical performance for different hardware implementations. The selection of frame-based vision systems is based on the work of Ye [22]. The performance indicators K_{lat} and K_{smp} are defined in Eqs. (9) and (10). *Although the EVK4 camera sensor has 720x1280 pixels, we define a range-of-interest of a circle of 210 pixels in radius. † The latency is composed of 3.6 ms related to the USB data transfer from the event camera to the desktop computer, and 1.2 ms related to the event camera sensor and tracking algorithm (as explained in Suppl. Sec. 5.2).

Pixels n_{pix}	Latency τ_{lat} (ms)	Sample rate f_{smp} (Hz)	K_{lat} (kpix/ms)	K_{smp} (kpix/ms)	Processing unit	Camera data	Tracking application	Source
3600	0.16	6000	23	22	FPGA	Frames	Bird wing motion analysis	Graetzel [36]
160x100	1	1600	16	26	FPGA	Frames	1-dof motion control	Ye [22]
320x240	1	1000	77	77	FPGA	Frames	Pose estimation	Komuro [37]
640x480	9.8	283	31	87	FPGA & CPU	Frames	Object tracking	Liu et al. [23].
1600x1200	–	100	–	192	FPGA	Frames	Color image processing	Harvilov [38]
768x576	–	33–50	–	22	CPU	Frames	Color image processing	Johnsen et al. [20]
128x128	2.8	–	5.9	–	CPU	Events	Goalkeeper	Dellbruck et al. [25]
128x128	–	4000	–	66	CPU	Events	Haptic feedback gripper	Ni et al. [27]
138544*	$1.2+3.6^{\dagger}$	2000	29	276	CPU	Events	1-dof motion control	This work

$$K_{\text{lat}} = \frac{n_{\text{pix}}}{\tau_{\text{lat}}} \tag{9}$$

$$K_{\text{smp}} = n_{\text{pix}} \cdot f_{\text{smp}} = \frac{n_{\text{pix}}}{\tau_{\text{smp}}}, \tag{10}$$

where n_{pix} equals the number of pixels, τ_{lat} the latency (time after which the tracking information is available), f_{smp} the sample frequency of the vision system and τ_{smp} the time interval between tracking data points. The sample frequency f_{smp} is related to the sample interval τ_{smp} using $\tau_{\text{smp}} = \frac{1}{f_{\text{smp}}}$.

The vision tracking presented in this work has comparable values for K_{lat} and K_{smp} as the frame-based vision systems listed in Table 4. However, the event camera uses USB 3.0 to transfer event-data to the desktop PC which causes the main part (3.6 ms) of the delay τ_{lat}. This delay can be reduced by tuning the USB protocol or using a different connection [35], which would result in a higher value for K_{lat}. Moreover, in our implementation the tracking algorithm is implemented on a desktop computer. The performance of this computer limits the sample rate at which the tracking algorithm can be executed to 2 kHz. The delay related to the tracking algorithm equals two sample periods ($2 \cdot \tau_{\text{smp}} = 1$ ms), as explained in Suppl. Sec. 5.2. Nevertheless, Liu [23] has shown that object tracking implemented on an FPGA can be 20 times faster compared to implementation on the CPU of a desktop computer. Therefore, we expect that the performance of our tracking system would be higher in terms of K_{lat} and K_{smp} if the tracking algorithm would be implemented on an FPGA.

It is advantageous for a feedback system to have a low tracking latency, as this yields less phase lag according to $\phi = \tau_{\text{d}} f_{\text{c}} \cdot 360$. Less phase lag results in a higher phase margin (Suppl. Fig. 9b and Table 2) of the controlled system and thus more damping ($\zeta \approx \text{PM}/100$). Alternatively, it would allow us to increase the cross-over frequency f_{c} while retaining the phase margin. Consequently, a higher cross-over frequency f_{c} would result in a stiffer response (see Suppl. Sec. 3.1).

Outlook

The feedback implementation shown in this work can be improved in several aspects. First, we expect that more information can be extracted from the tracking output. The spreading of events in each accumulation interval could give information about the velocity of the tracked object, as it is related to the traversed distance during the accumulation period. Alternatively, negative events could be tracked separately to provide additional information about the object position and movement direction.

Second, state feedback [19] could be implemented, which is a more thorough controller design approach than designing a controller in the frequency domain. However, this requires velocity information of the particle, as well as a more thorough identification of the system.

Third, also the vertical motion of the levitated particle can be controlled using position feedback. This would allow for two-dimensional position control of the levitated particle and further reduce vertical vibrations. However, the eigenfrequency $f_{\text{n-z}}$ is at 39 Hz, which is about three times higher than the horizontal eigenfrequency $f_{\text{n-x}}$. At 39 Hz, the phase lag due to the system delay (Table 1) equals $\phi = \tau_{\text{d}} f \cdot 360 = 75°$, which limits the possibilities of PID control which requires a positive phase margin of about 30°. Finally, the motion in all directions could be tracked by adding a second event camera. This would allow to stabilize the motion of the particle in all directions.

5. Conclusion

In this work we show that a levitated particle can be stabilized using feedback control. We show how an event camera can be used to track the position of a particle in real-time, and how to implement the camera as a sensor in a feedback loop. We make

clear that using an event camera a higher sample rate f_{smp} or more pixels can be used with respect to a frame-based camera, as the pixel-sample rate product K_{smp} Eq. (10) of 276 is the highest of all listed vision systems in Table 4. Subsequently, we show how to identify the dynamics of the levitated particle and how to design a PID controller that stabilizes the particle position. The performance of the controller can be predicted by the model and therefore be tuned to specific performance targets. We show that using position feedback, the RMS value of the vibrations in horizontal direction (σ_x) is reduced from 1.0×10^{-4} m to 1.9×10^{-5} m and the settling time T_s is reduced from 2.3 s to 6×10^{-2} s. In this way we contribute to the usability of acoustic levitation by tackling the inherent challenges like long response time [11] and vibrations due to disturbances. With the feedback control, the positioning precision of acoustic levitation is brought into a regime comparable to the positioning performance of additive manufacturing methodologies [6].

We note that the presented procedure can be implemented as well to stabilize other (levitated) objects. The optical setup can be adjusted to visualize structures ranging from macro to micro scale. In this way even for small-scale systems (which are usually very difficult to track) the position can be stabilized and controlled with micrometer precision. This could open up new possibilities in the field of microassembly.

CRediT authorship contribution statement

Vincent Bos: Writing – original draft, Visualization, Validation, Methodology, Conceptualization; **Mohamed El Shenawy:** Methodology; **Jasper Wesselingh:** Supervision, Methodology, Conceptualization; **Peter G. Steeneken:** Writing – review & editing, Supervision, Project administration; **Gerard J. Verbiest:** Writing – review & editing, Supervision.

Declaration of competing interest

The authors declare the following financial interests/personal relationships which may be considered as potential competing interests:

Peter G. Steeneken reports financial support was provided by Netherlands Enterprise Agency. If there are other authors, they declare that they have no known competing financial interests or personal relationships that could have appeared to influence the work reported in this paper.

Acknowledgement

We thank John Fearnhead for improving the fluency of English in the manuscript, Aditya Natu for his critical remarks on mathematical expressions and Frederike Wörtche and Ruben Guis for helping with formatting the references. This work is financed by ITEC B.V. and co-financed by the Netherlands Enterprise Agency (RVO).

Data availability

Data will be made available on request.

Supplementary material

Supplementary material associated with this article can be found in the online version at 10.1016/j.jsv.2026.120040.

References

[1] F. Priego-Capote, L. de Castro, Ultrasound-assisted levitation: lab-on-a-drop, TrAC Trends Anal. Chem. 25 (9) (2006) 856–867. https://doi.org/10.1016/j.trac.2006.05.014
[2] S. Santesson, S. Nilsson, Airborne chemistry: acoustic levitation in chemical analysis, Anal. Bioanal. Chem. 378 (7) (2004) 1704–1709. https://doi.org/10.1007/s00216-003-2403-2
[3] A. Scheeline, R.L. Behrens, Potential of levitated drops to serve as microreactors for biophysical measurements, Biophys. Chem. 165–166 (2012) 1–12. https://doi.org/10.1016/j.bpc.2012.03.008
[4] V. Vandaele, A. Delchambre, P. Lambert, Acoustic wave levitation: handling of components, J. Appl. Phys. 109 (12) (2011) 124901. https://doi.org/10.1063/1.3594245
[5] V. Vandaele, P. Lambert, A. Delchambre, Non-contact handling in microassembly: acoustical levitation, Precis. Eng. 29 (4) (2005) 491–505. https://doi.org/10.1016/j.precisioneng.2005.03.003
[6] Q. Qin, Z. Cheng, C. Wen, J. Huang, 3D Printing on droplets by ultrasonic levitation, Addit. Manuf. Front. 4 (2) (2025) 200206. https://doi.org/10.1016/j.amf.2025.200206
[7] C.R.P. Courtney, C.E.M. Demore, H. Wu, A. Grinenko, P.D. Wilcox, S. Cochran, B.W. Drinkwater, Independent trapping and manipulation of microparticles using dexterous acoustic tweezers, Appl. Phys. Lett. 104 (15) (2014) 154103. https://doi.org/10.1063/1.4870489
[8] A. Marzo, A. Barnes, B.W. Drinkwater, TinyLev: a multi-emitter single-axis acoustic levitator, Rev. Sci. Instrum. 88 (8) (2017) 085105. https://doi.org/10.1063/1.4989995
[9] C. Andersson, Acoustic levitation of multi-wavelength spherical bodies using transducer arrays of non-specialized geometries, J. Acoust. Soc. Am. 151 (5) (2022) 2999–3006. https://doi.org/10.1121/10.0010358
[10] A. Marzo, S.A. Seah, B.W. Drinkwater, D.R. Sahoo, B. Long, S. Subramanian, Holographic acoustic elements for manipulation of levitated objects, Nat. Commun. 6 (1) (2015) 8661. Number: 1 Publisher: Nature Publishing Group. https://doi.org/10.1038/ncomms9661
[11] V. Bos, J. Wesselingh, G.J. Verbiest, P.G. Steeneken, Active damping for acoustic levitation in air, AIP Adv. 14 (9) (2024) 095009. https://doi.org/10.1063/5.0210800
[12] R. Malkin, B. Kappus, B. Long, A. Price, On the non-linear behaviour of ultrasonic air-borne phased arrays, J. Sound Vib. 552 (2023) 117644. https://doi.org/10.1016/j.jsv.2023.117644

[13] M.W. Mooiweer, Visualisation of ultrasound waves in air to support acoustic levitation (2023). https://repository.tudelft.nl/record/uuid:361721a1-6d4b-4e84-811d-7860832c662f.
[14] F.S.L. Wörtche, F. Maucher, M. Mooiweer, G.J. Verbiest, P.G. Steeneken, Characterizing ultrasonic standing wave fields by Schlieren imaging, Ultrasonics 156 (2025) 107743. https://doi.org/10.1016/j.ultras.2025.107743
[15] A. Pavlic, J. Dual, On the streaming in a microfluidic Kundt's tube, J. Fluid Mech. 911 (2021) A28. https://doi.org/10.1017/jfm.2020.1046
[16] C.P. Lee, T.G. Wang, Outer acoustic streaming, J. Acoust. Soc. Am. 88 (5) (1990) 2367–2375. https://doi.org/10.1121/1.400079
[17] M.A.B. Andrade, N. Pérez, J.C. Adamowski, Review of progress in acoustic levitation, Braz. J. Phys. 48 (2) (2018) 190–213. https://doi.org/10.1007/s13538-017-0552-6
[18] M.A.B. Andrade, S. Zehnter, F. Funke, C. Ament, Model-based feedforward control for an optimized manipulation of acoustically levitated spheres, AIP Adv. 14 (4) (2024) 045033. https://doi.org/10.1063/5.0202967
[19] R. M. Schmidt, G. Schitter, A. Rankers, J. van Eijk, High Performance Mechatronics, IOS Press, 2nd edition, 2014.
[20] S. Johnsen, A. Tews, Real-time object tracking and classification using a static camera, in: Proceedings of the IEEE ICRA 2009 Workshop on People Detection and Tracking, 2009.
[21] C.E. Willert, Event-based imaging velocimetry using pulsed illumination, Exp. Fluids 64 (5) (2023) 98. https://doi.org/10.1007/s00348-023-03641-8
[22] Z. Ye, Implementation, Modeling, and Exploration of Precision Visual Servo Systems, Phd Thesis 1 (Research TU/e / Graduation TU/e), Technische Universiteit Eindhoven, Eindhoven, 2020.
[23] S. Liu, A. Papakonstantinou, H. Wang, D. Chen, Real-time object tracking system on FPGAs, in: 2011 Symposium on Application Accelerators in High-Performance Computing, 2011, pp. 1–7. https://doi.org/10.1109/SAAHPC.2011.22
[24] P.I. Corke, M.C. Good, Dynamic effects in visual closed-loop systems, IEEE Trans. Robot. Autom. 12 (5) (1996) 671–683. https://doi.org/10.1109/70.538973
[25] P. Lichtsteiner, C. Posch, T. Delbruck, A 128 X 128 120db 30mw asynchronous vision sensor that responds to relative intensity change, in: 2006 IEEE International Solid State Circuits Conference - Digest of Technical Papers, 2006, pp. 2060–2069. https://doi.org/10.1109/ISSCC.2006.1696265
[26] T. Delbruck, Frame-free dynamic digital vision, in: Proceedings of Intl. Symp. on Secure-Life Electronics, Advanced Electronics for Quality Life and Society, Univ. of Tokyo, Mar. 6–7, 2008, 2008, pp. 21–26.
[27] Z. Ni, A. Bolopion, J. Agnus, R. Benosman, S. Regnier, Asynchronous event-based visual shape tracking for stable haptic feedback in microrobotics, IEEE Trans. Robot. 28 (5) (2012) 1081–1089. https://doi.org/10.1109/TRO.2012.2198930
[28] G. Gallego, T. Delbrück, G. Orchard, C. Bartolozzi, B. Taba, A. Censi, S. Leutenegger, A.J. Davison, J. Conradt, K. Daniilidis, D. Scaramuzza, Event-based vision: a survey, IEEE Trans. Pattern Anal. Mach. Intell. 44 (1) (2022) 154–180. https://doi.org/10.1109/TPAMI.2020.3008413
[29] H.K. Yuen, J. Princen, J. Illingworth, J. Kittler, et al., Comparative study of Hough transform methods for circle finding, Image Vis. Comput. 8 (1) (1990) 71–77. https://doi.org/10.1016/0262-8856(90)90059-E
[30] Prophesee, Spatter tracking using C++ — metavision SDK docs 4.6.2 documentation, 2024, https://docs.prophesee.ai/stable/samples/modules/analytics/tracking_spatter_cpp.html.
[31] B.F. Barreiros, J.O. Trierweiler, M. Farenzena, Reliable and straightforward PID tuning rules for highly underdamped systems, Braz. J. Chem. Eng. 38 (4) (2021) 731–745. https://doi.org/10.1007/s43153-021-00127-0
[32] G.F. Franklin, J.D. Powell, A. Emami-Naeini, Feedback Control of Dynamic Systems, Pearson Education, 6 edition, 2010.
[33] N. Sugita, T. Oshino, T. Shinshi, Nonlinear coupling between radial and axial vibrations during single-axis acoustic levitation in mid-air, Int. J. Mech. Sci. 246 (2023) 108159. https://doi.org/10.1016/j.ijmecsci.2023.108159
[34] S.A. Seah, B.W. Drinkwater, T. Carter, R. Malkin, S. Subramanian, Correspondence: dexterous ultrasonic levitation of millimeter-sized objects in air, IEEE Trans. Ultrason. Ferroelectr. Freq. Control 61 (7) (2014) 1233–1236. https://doi.org/10.1109/TUFFC.2014.3022
[35] Prophesee, Transfer latency, 2025. https://support.prophesee.ai/portal/en/kb/articles/evk-latency.
[36] C.F. Graetzel, S.N. Fry, B.J. Nelson, A 6000 Hz computer vision system for real-time wing beat analysis of drosophila, in: The First IEEE/RAS-EMBS International Conference on Biomedical Robotics and Biomechatronics, 2006. BioRob 2006., 2006, pp. 278–283. https://doi.org/10.1109/BIOROB.2006.1639099
[37] T. Komuro, A. Iwashita, M. Ishikawa, A QVGA-size pixel-parallel image processor for 1,000-fps vision, IEEE Micro 29 (6) (2009) 58–67. https://doi.org/10.1109/MM.2009.89
[38] D. Havrilov, S. Baraban, A. Volovyk, O. Zviahin, A. Semenov, A. Savytskyi, Real-time video processing system based on field programmable gate array, in: 2019 IEEE 14th International Conference on Computer Sciences and Information Technologies (CSIT), 2, 2019, pp. 192–196. https://doi.org/10.1109/STC-CSIT.2019.8929758